Practical Photonic Quantum Sensing with Thermal Light

Peng Kian Tan[1],* Xi Jie Yeo[1], Alvin Zhen Wei Leow[2], Lijiong Shen[1], and Christian Kurtsiefer[1,2]
[1] *Centre for Quantum Technologies, 3 Science Drive 2, Singapore 117543 and*
[2] *Department of Physics, National University of Singapore, 2 Science Drive 3, Singapore, 117542*
(Dated: March 20, 2023)

Quantum sensing exploits quantum phenomena to improve the measurements of physical parameters and can be implemented in photonic, atomic or solid-state systems[1]. Photonic quantum sensing techniques include ghost imaging and super-resolution imaging[2]. Many photonic quantum sensing schemes rely on photon pairs generated in spontaneous parametric down conversion (SPDC)[3] that can be entangled in several degrees of freedom, but most often make use of the temporal correlation between the photons[4]. Examples are range finding[5,6] and clock synchronization[7,8] schemes, where quantum light sources have an advantage of being stationary, and therefore carrying no obvious timing structure that may be subject to manipulation or eavesdropping. The luminosity of SPDC-based photon pair sources is typically limited to sub-nanowatts. In this work, we consider thermal light an alternative resource of time-correlated photons by exploiting its photon bunching property. We demonstrate quantum sensing using a relatively simple thermal light source with an optical power of about 12.5 μW and a spectral linewidth around 43 MHz in a single optical mode. The resulting spectral density of this source exceeds that of SPDC sources by approximately 10 orders of magnitude. We demonstrate its usefulness in an optical ranging experiment over about 1.8 km.

Time-correlated photon pairs Photonic sensing applications often make use of modulated light sources and seek for correlations of a returned signal with the modulation. In an attempt of moving to low light levels, one can make use of inherent temporal correlations found in photon pairs emerging from a spontaneous parametric down conversion (SPDC) process in crystals with second-order non-linear optical response, or through four-wave mixing (FWM) in optical fibers or atomic vapours. These processes generate pairs of photons that exhibit a strong correlation of photodetection events, manifesting in a strongly peaked second order correlation function $g^{(2)}(\tau) = f(\tau/\tau_c)$, which characterizes a probability to observe a pair at a time difference τ. The function f is strongly peaked around $\tau = 0$ (with a spread on the order of a coherence time τ_c), and is of inherent quantum nature, and can be observed in specialized quantum light sources. Sensing applications based on this effect are carried out by measuring detection time differences between one photon acting as a reference, and the other one acting as a probe.

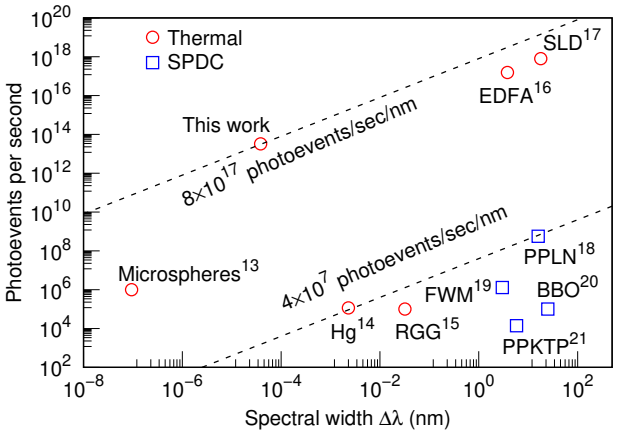

FIG. 1. Spectral densities of thermal and SPDC light sources based on: Microspheres[13] – suspension of microspheres, Hg[14] – Mercury discharge lamp, RGG[15] – rotating ground glass, EDFA[16] – Erbium-doped fiber amplifier, SLD[17] – superluminescent diode, PPLN[18] – periodically poled Lithium Niobate, FWM[19] – four-wave mixing, BBO[20] – Beta-Barium Borate, PPKTP[21] – periodically poled Potassium Titanyl Phosphate.

A more natural type of light is thermal light. Thermal light, such as blackbody radiation, exhibits a characteristic temporal photon bunching behavior[9,10], also known as the Hanbury-Brown–Twiss effect[11]. This is also described by a peaked second-order timing correlation,

$$g^{(2)}(\tau) = 1 + e^{-2|\tau|/\tau_c}\,, \tag{1}$$

where τ is again the timing separation of the two photodetection events, and τ_c is the coherence timescale of the temporal photon bunching where thermal photons have a tendency to propagate closer together than described by Poissonian statistical timing distribution. Similar to light generated by SPDC, the coherence timescale τ_c is inversely proportional to the spectral width $\Delta\lambda$ of the thermal light, which is given by the Fourier transform of the source power spectrum[12], such that $\Delta\lambda = 1/\tau_c$ for single-line Gaussian spectrum.

An important practical consideration for sensing applications is the brightness of the correlated light source. As shown in Fig. 1, SPDC light sources generate an output power below a nanowatt, or in the range of 10^4 to 10^9

* cqttpk@nus.edu.sg

photoevents per second. This limits the practicality of SPDC light-based sensing in environments with high attenuation or loss. Another important property in a temporal correlation measurement is the accuracy that can be practically used infer e.g. a time-of-flight for one of the photons. Timing uncertainties of semiconductor-based single-photon detectors are somewhere below a nanosecond, but more recent nanowire-based detectors may reach a few picoseconds. When identifying the temporal correlation feature in thermal light, however, it is necessary that the correlation peak is still detectable. If the coherence time of the thermal light is significantly smaller than the detector timing uncertainty, the visibility of the temporal correlation washes out and may make it impossible to identify it on top of the Poissonian background. It is therefore desirable to use thermal light sources with a spectral width below $\approx 1\,\mathrm{GHz}$.

Thermal light with such a narrow optical bandwidth has been generated in many different ways. Early examples include single emission lines of gas discharge lamps. Other methods involve transmitting laser light through random dispersion media such as suspension of microspheres, or a rotating ground glass plate. These sources, however, have either relatively low output power due to the spatial incoherence of the randomization mechanism, or (e.g. in the case of rotating ground glass modulators) a relatively long coherence time.

In this work, we use a laser diode operating below the lasing threshold[22,23] to generate thermal light[24,25]. This amplified spontaneous emission process generates significantly higher output power in the range of $10\,\mu\mathrm{W}$ to $100\,\mathrm{mW}$. Light sources of a similar category include superluminescent diodes, and Erbium-doped fiber amplifiers. These examples tend to have spectral densities above milliwatts per nanometer.

Quantum sensing setup The stationary thermal light generated from a subthreshold laser diode is implemented into an optical ranging setup based on time-of-flight measurements, commonly known as light distance and ranging (lidar).

While conventional lidar introduces timing modulation[26,27] into the intensity, amplitude, or phase of the light source, to provide timing correlations, this work exploits the temporal photon bunching of thermal light to provide the timing correlations.

The lidar configuration illustrated in Fig. 2 is based on increasing the coherence timescale of the thermal light by narrowband spectral filtering[28], and then performing coincidence measurements with high timing resolution to record the temporal photon bunching signature $g^{(2)}(\tau)$.

The $g^{(2)}$ photon bunching peak is shifted by a time τ_0 in its timing position, corresponding to the optical path length difference between probe and reference beam, thus allowing to infer the distance of a target retroreflector from the peak position of $g^{(2)}$ and the speed of light.

The stationary light source in our demonstration is a laser diode operating at a subthreshold current of

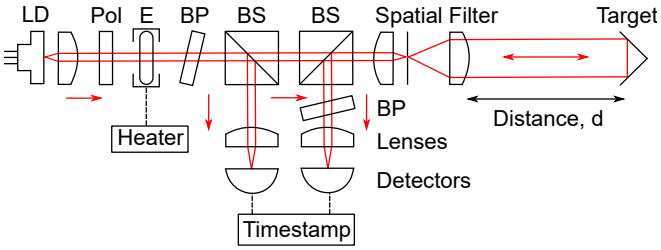

FIG. 2. The experimental setup using thermal light to perform ranging measurements. LD: laser diode, Pol: polariser, E: etalon, BP: bandpass filter, BS: beamsplitter.

32.9 mA which is determined in Fig. 5 via the output power and spectrum, and therefore exhibits the photon bunching behaviour that is characteristic of thermal light.

The thermal light is first sent through a single-mode optical fiber to select for the fundamental Gaussian mode to enforce spatial coherence, then transmitted through a polarizer to obtain a well-defined linear polarization, and spectrally filtered by an etalon (see Methods section for details).

An asymmetric beamsplitter directs 92 % of the filtered thermal light into the probe beam and retains 4 % as a local reference beam sent to a first single photon detector. After some spatial beam conditioning (see Methods section), the probe beam propagats to the retroreflector target, and back to the sensing setup onto the second single photon detector.

Both single photon detectors are actively quenched Silicon avalanche photodiodes with a quantum efficiency about 50 % at 550 nm and a timing jitter around 40 ps. The detected photoevents are timestamped either by an oscilloscope with (sampling rate 40 GSPS), and time differences were histogrammed into 40 ps wide time bins, through an FPGA-based timestamp device into 2 ns wide time bins.

Range sensing demonstration Figure 3 shows two time difference histograms together with a fitted second-order timing correlation function $g^{(2)}(\tau)$ according to Eqn. 1 that allows to determine the positions τ_0 of their respective bunching peaks, and the corresponding ranging distance d extracted from the round trip time of the probe beam for a set of target placement positions(Fig. 3, bottom trace). The resulting ranges are in good agreement with their corresponding target placement positions, and compatible with a constraint in the detector timing jitter (about 40 ps FWHM).

To demonstrate the robustness of the ranging setup in a real-world environment, we conducted two outdoor field measurements in Downtown Singapore.

Time-of-flight measurements in Fig. 4 are compared between a reference zero position (black) and outfield locations, resulting in the ranging distances of $96529 \pm 2\,\mathrm{cm}$ (blue) and $185148 \pm 2\,\mathrm{cm}$ (red) fitted to Eqn. 1 with reduced χ^2 of 1.09 and 1.05, respectively, under the as-

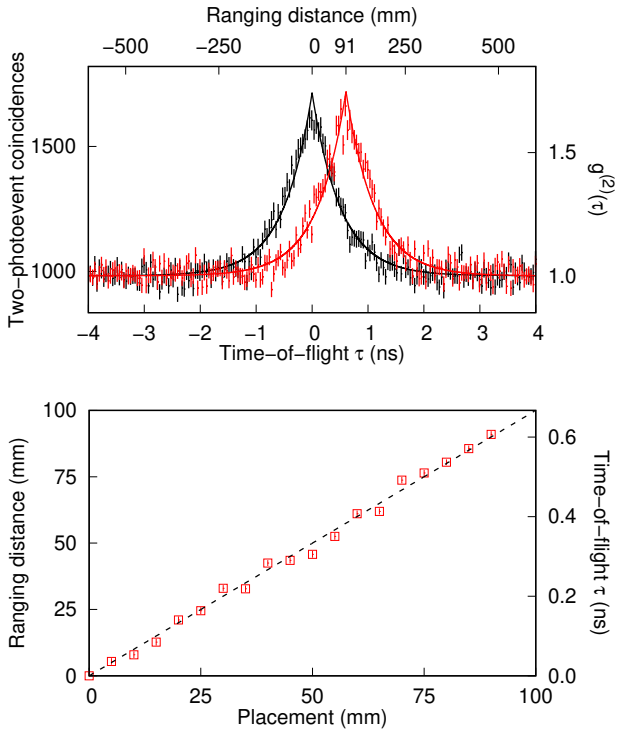

FIG. 3. [Top]: The photon bunching $g^{(2)}(\tau)$ measurements with the target reflector placed at 0 mm (black) and 90 mm (red). The solid line represents a fit to Eqn. 1 resulting in $\tau_c = 1.03\pm0.03$ ns, a peak displacement of $\tau_0 = 0.606\pm0.008$ ns corresponding to a ranging distance of d=91.0±1.2 mm, with a reduced χ^2 of 1.19. [Bottom]: The fitted ranging distances are plotted against their placement positions to test for dstance resolution.

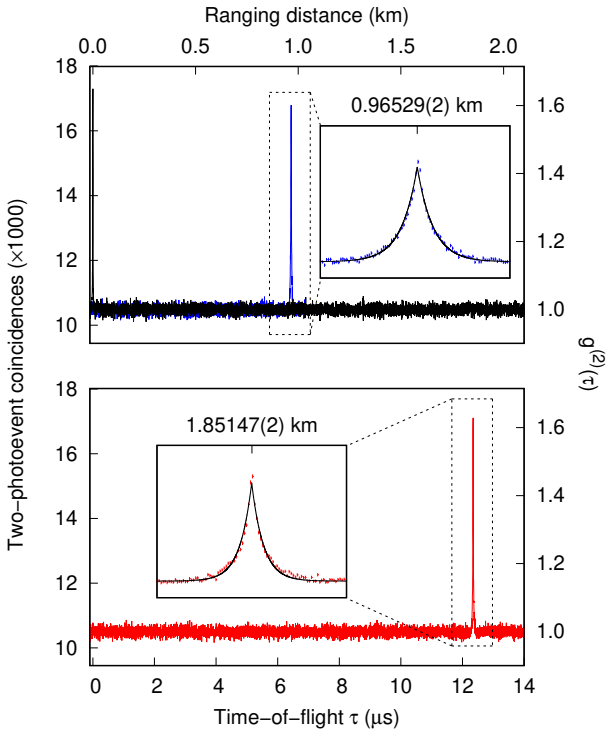

FIG. 4. Optical ranging measurements to the reference zero distance position with the retroreflector placed at the telescope aperture, and to the target retroreflector located at kilometric distances.

sumption of a unit refractive index of air. The increased uncertainty compared to the short range measurements shown in 3 are due to the more coarse histogramming for this experiment.

For these measurements, the etalon temperature tuning and stability was improved relative to the measurements in Fig. 3, increasing the coherence timescale $\tau_c = 23.2 \pm 0.4$ ns (red), corresponding to a spectral linewidth $\Delta\lambda = 43$ MHz.

The temporal photon bunching peak (red) is slightly reduced to $g^{(2)}(\tau = 0) = 1.591 \pm 0.009$ (red) due to an increase of the bin width from 40 ps to 2 ns for the time differences, and by noise contribution from ambient light to the probe detector.

The very high spectral density of our light source of 12.5 μW in a 43 MHz spectral band increases the signal-to-noise ratio[29,30] of a bunching peak detection significantly. Even for an attenuation or loss of 65 dB in the probe path, the actively quenched Silicon avalanche photodetectors could be saturated (see Methods section for more details).

Quantum sensing using thermal light This work explored the use of thermal light for applications where measurements (like range finding) are based on detecting correlations in time are at the core of the sensing task. Sub-threshold lasers and a narrowband filtering technique helped to provide a powerful alternative to light sources based on spontaneuous parametric down conversion in quantum sensing applications that may offer superior signal-to-noise ratios, at a much reduced system complexity.

With such light sources, we envision that a technique originally used for estimating the size of stars half a century ago can boost a wide range of practical quantum sensing applications that mostly rely on temporal correlations.

Acknowledgments This research is supported by the Quantum Engineering Programme through NRF2021-QEP2-03-P02, the Ministry of Education and the National Research Foundation, Prime Minister's Office, Singapore.

1. S. Pirandola, B. R. Bardhan, T. Gehring, C. Weedbrook, and S. Lloyd, Advances in photonic quantum sensing, Nat. Photonics **12**, 724 (2018).
2. P.-A. Moreau, E. Toninelli, T. Gregory, and M. J. Padgett, Imaging with quantum states of light, Nature Reviews Physics **1**, 367 (2019).
3. R. Ghosh and L. Mandel, Observation of nonclassical effects in the interference of two photons, Phys. Rev. Lett. **59**, 1903 (1987).
4. A. S. Clark, M. Chekhova, J. C. F. Matthews, J. G. Rarity, and R. F. Oulton, Special topic: Quantum sensing with correlated light sources, Appl. Phys. Lett. **118**, 060401 (2021).
5. E. D. Lopaeva, I. R. Berchera, I. P. Degiovanni, S. Olivares, G. Brida, and M. Genovese, Experimental realization of quantum illumination, Phys. Rev. Lett. **110**, 153603 (2013).
6. S. Barzanjeh, S. Guha, C. Weedbrook, D. Vitali, J. H. Shapiro, and S. Pirandola, Microwave quantum illumination, Phys. Rev. Lett (2015).
7. C. Ho, A. Lamas-Linares, and C. Kurtsiefer, Clock synchronization by remote detection of correlated photon pairs, New J. Phys. **11**, 045011 (2009).
8. J. Lee, L. Shen, A. Cere, J. Troupe, A. Lamas-Linares, and C. Kurtsiefer, Symmetrical clock synchronization with time-correlated photon pairs, Appl. Phys. Lett. **114**, 101102 (2019).
9. R. Glauber, The quantum theory of optical coherence, Phys. Rev. **130**, 2529 (1963).
10. R. Glauber, Coherent and incoherent states of the radiation field, Phys. Rev. **131**, 2766 (1963).
11. R. Hanbury-Brown and R. Q. Twiss, Correlation between photons in two coherent beams of light, Nature **177**, 27 (1956).
12. M. Fox, *Quantum Optics: An Introduction* (Oxford University Press, UK, 2006).
13. D. Dravins, T. Lagadec, and P. D. Nunēz, Optical aperture synthesis with electronically connected telescopes, Nat. Commun. **6**, 6852 (2015).
14. P. K. Tan, A. H. Chan, and C. Kurtsiefer, Optical intensity interferometry through atmospheric turbulence, MNRAS **457**, 4291 (2016).
15. J. Zhu, X. Chen, P. Huang, and G. Zeng, Thermal-light-based ranging using second-order coherence, Appl. Opt. **51**, 4885 (2012).
16. P. Janassek, A. Herdt, S. Blumenstein, and W. Elsaber, Ghost spectroscopy with classical correlated amplified spontaneous emission photons emitted by an erbium-doped fiber amplifier, Appl. Sci. **8(10)**, 1896 (2018).
17. A. T. M. A. Rahman and P. F. Barker, Optical levitation using broadband light, Optica **7(8)**, 906 (2020).
18. Z. Zhang, S. Mouradian, F. N. C. Wong, and J. Shapiro, Entanglement enhanced sensing in a lossy and noisy environment, Phys. Rev. Lett. **114**, 110506 (2015).
19. D. G. England, B. Balaji, and B. J. Sussman, Quantum-enhanced standoff detection using correlated photon pairs, Phys. Rev. A **99**, https://doi.org/10.1103/PhysRevA.99.023828 (2019).
20. A. Lohrmann, A. Villar, A. Stolk, and A. Ling, High fidelity yield stop collection for polarization-entangled photon pair sources, Appl. Phys. Lett. **113**, 171109 (2018).
21. Y.-C. Jeong, K.-H. Hong, and Y.-H. Kim, Bright source of polarization-entangled photons using a ppktp pumped by a broadband multi-mode diode laser, Opt. Express **24(2)**, 1165 (2016).
22. M. G. A. Bernard and G. Duraffourg, Laser conditions in semiconductors, Physica Status Solidi B **1**, 699 (1961).
23. G. Lasher and F. Stern, Spontaneous and stimulated recombination radiation in semiconductors, Phys. Rev. **133** (1964).
24. W. Shockley and J. W. T. Read, Statistics of the recombinations of holes and electrons, Phys. Rev. **87** (1952).
25. D. T. Cassidy, Spontaneous-emission factor of semiconductor diode lasers, JOSA B **8**, 747 (1991).
26. G. Beheim and K. Fritsch, Range finding using frequency-modulated laser diode, Appl. Opt. **25**, 1439 (1986).
27. S. Royo and M. Ballesta-Garcia, An overview of lidar imaging systems for autonomous vehicles, Appl. Sci. **9**, 4093 (2019).
28. P. K. Tan and C. Kurtsiefer, Temporal intensity interferometry for characterization of very narrow spectral lines, MNRAS **469**, 1617 (2017).
29. R. Hanbury-Brown, *The Intensity Interferometer: Its Application To Astronomy* (Taylor & Francis ; Halsted Press, London ; New York, 1974) p. 184.
30. C. Foellmi, On the intensity interferometry and the second-order correlation function $g^{(2)}$ in astrophysics, A&A **507**, 1719 (2009).
31. P. K. Tan, G. H. Yeo, H. S. Poh, A. H. Chan, and C. Kurtsiefer, Measuring temporal photon bunching in blackbody radiation, ApJL **789**, L10 (2014).

Methods

Subthreshold laser diode Laser diodes generate coherent laser light with Poissonian timing statistics when operating above the lasing threshold current. Below threshold, the optical spectrum and power resemble that of light emitting diodes, with a thermal photon statistics.

For our device (nominal lasing wavelength $\lambda = 518\,\mathrm{nm}$, single-mode spatial output), the lasing threshold current was found to be around 33 mA (see Fig. 5), where the output power exhibits a sharp increase of 3 orders of magnitude, and the spectrum narrows to a single emission line, limited by the grating spectrometer to about 0.3 nm.

The thermal light generated at a subthreshold current of 32.9 mA is coupled into a single spatial mode of an optical fiber, resulting in a very bright spectral density of around $12.5\,\mu\mathrm{W}$, corresponding to approximately 10^{13} photoevents per second, within a spectral width $\Delta\lambda = 43\,\mathrm{MHz}$.

Thermal light preparation To select a relatively narrow window of thermal light from the spectrum emitted by the sub-threshold laser source, a combination of a band passfilter (BP in Fig. 2) and a etalon is used. The etalon is based on a Fused Silica (Suprasil311) substrate with reflective coatings of 97 % on both sides for a corresponding reflectivity finesse of 103. The plano-parallel substrate has a thickness of 0.5 mm, resulting in a recip-

rocal free spectral range of about 205 GHz, to suppress the laser diode chip modes of about 50 GHz separation.

The passband of the etalon has a full width at half maximum of 2 GHz[31]. While the subthreshold spectral linewidth of 43 MHz is already narrower than the etalon passband, the subthreshold spectrum shows multiple laser cavity modes, which we reduce to one with the etalon, which is temperature-tuned with a slope of 4 GHz/K. The bandpass interference filter BP has a 2 nm wide passband centred at $\lambda = 518$ nm to suppress source light beyond the free spectral range of the etalon, as well as to block ambient light from illuminating the probe detector.

Spatial light conditioning The spectrally filtered thermal light beam passes through a 50:50 beamsplitter and a telescope formed by a lens pair (f=50 mm, f=300 mm) around a spatial filter, and is expanded to a diameter of about 50 mm. The probe beam returns from the target reflector through the same telescope and beam splitter onto the probe photodetector. The spatial filter cleans up the returning probe beam and reduces ambient light contribution from reaching the detectors, and the use of a second beam splitter ensures that no breakdown flash light from the target detector can reach the reference photodetector.

Signal-to-noise ratio In the regime whereby the photodetectors are fast enough to resolve the temporal coherence τ_c of the photon bunching signal, the measurable $g^{(2)}(\tau)$ signal-to-noise ratio (SNR) can be described by:

$$\mathrm{SNR} = r \cdot V^2 \sqrt{\tau_c \cdot \Delta T}\,, \tag{2}$$

with the rate r in photoevents per second, the interferometric visibility $V = \sqrt{g^{(2)}(0) - 1}$, the coherence time τ_c in seconds, and the integration time ΔT in seconds.

Considering the output power of 12.5 μW of the subthreshold laser diode at 32.9 mA, an attenuation loss of -65 dB will result in the photodetectors still being saturated at about $r = 10^7$ photoevents per second.

Using a photon bunching peak value $V^2 = 0.6$ and a coherence timescale $\tau_c = 23$ ns, which corresponds to the measured values in Fig. 4, an upper-bound signal-to-noise ratio of around 30 may be achieved within just 1 millisecond of integration time ΔT.

This high tolerance to attenuation upwards of -65 dB provides the thermal light source an advantage over SPDC light sources in practical sensing use-cases whereby significant losses can be expected.

Extended data

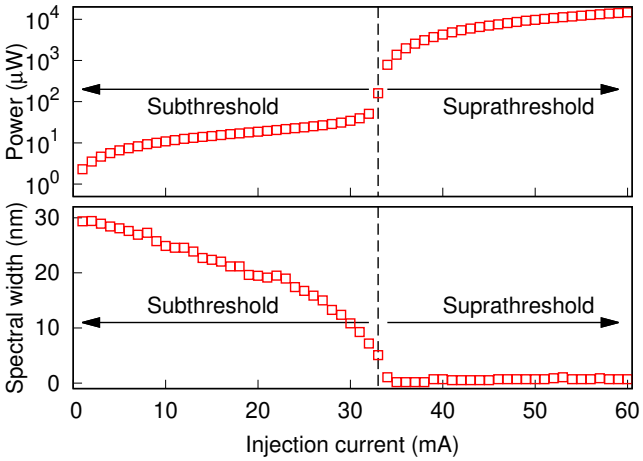

FIG. 5. The output power and spectral width $\Delta\lambda$ of a laser diode are measured against its injection current to determine the lasing threshold.